HHS Public Access

Author manuscript

J Magn Reson Imaging. Author manuscript; available in PMC 2021 May 01.

Published in final edited form as:

J Magn Reson Imaging. 2020 May ; 51(5): 1357–1368. doi:10.1002/jmri.26986.

Parametric Hemodynamic 4D Flow MRI Maps for the Characterization of Chronic Thoracic Descending Aortic Dissection

Kelly Jarvis, PhD[1,*], **Judith T. Pruijssen, MD**[2], **Andre Y. Son, MD**[3], **Bradley D. Allen, MD**[1], **Gilles Soulat, MD, PhD**[1], **Alireza Vali, PhD**[1], **Alex J. Barker, PhD**[4], **Andrew W. Hoel, MD**[5], **Mark K. Eskandari, MD**[5], **S. Chris Malaisrie, MD**[3], **James C. Carr, MD**[1], **Jeremy D. Collins, MD**[6], **Michael Markl, PhD**[1]

[1]Department of Radiology, Feinberg School of Medicine, Northwestern University, Chicago, Illinois, USA; [2]Department of Radiology and Nuclear Medicine, Radboud University Medical Centre, Nijmegen, The Netherlands; [3]Division of Cardiac Surgery, Feinberg School of Medicine, Northwestern University, Chicago, Illinois, USA; [4]Department of Radiology, University of Colorado, Denver, Colorado, USA; [5]Division of Vascular Surgery, Feinberg School of Medicine, Northwestern University, Chicago, Illinois, USA; [6]Department of Radiology, Mayo Clinic, Rochester, Minnesota, USA

Abstract

Background: Systematic evaluation of complex flow in the true lumen and false lumen (TL, FL) is needed to better understand which patients with chronic descending aortic dissection (DAD) are predisposed to complications.

Purpose: To develop quantitative hemodynamic maps from 4D flow MRI for evaluating TL and FL flow characteristics.

Study Type: Retrospective.

Population: In all, 20 DAD patients (age = 60 ± 11 years; 12 male) (six medically managed type B AD [TBAD], 14 repaired type A AD [rTAAD] now with ascending aortic graft [AAo] or elephant trunk [ET1] repair) and 21 age-matched controls (age = 59 ± 10 years; 13 male) were included.

Field Strength/Sequence: 1.5T, 3T, 4D flow MRI.

Assessment: 4D flow MRI was acquired in all subjects. Data analysis included 3D segmentation of TL and FL and voxelwise calculation of forward flow, reverse flow, flow stasis, and kinetic energy as quantitative hemodynamics maps.

Statistical Tests: Analysis of variance (ANOVA) or Kruskal–Wallis tests were performed for comparing subject groups. Correlation and Bland–Altman analysis was performed for the interobserver study.

[*]Address reprint requests to: K.J., Northwestern University Feinberg School of Medicine, Department of Radiology, 737 North Michigan Ave., Ste. 1600, Chicago, IL 60611. kelly.jarvis@northwestern.edu.

Results: Patients with rTAAD presented with elevated TL reverse flow (AAo repair: $P = 0.004$, ET1: $P = 0.018$) and increased TL kinetic energy (AAo repair: $P = 0.0002$, ET1: $P = 0.011$) compared to controls. In addition, TL kinetic energy was increased vs. patients with TBAD (AAo repair: $P = 0.021$, ET1: $P = 0.048$). rTAAD was associated with higher FL kinetic energy and lower FL stasis compared to patients with TBAD (AAo repair: $P = 0.002$, ET1: $P = 0.024$ and AAo repair: $P = 0.003$, ET1: $P = 0.048$, respectively).

Data Conclusion: Quantitative maps from 4D flow MRI demonstrated global and regional hemodynamic differences between DAD patients and controls. Patients with rTAAD vs. TBAD had significantly altered regional TL and FL hemodynamics. These findings indicate the potential of 4D flow MRI-derived hemodynamic maps to help better evaluate patients with DAD.

AORTIC DISSECTION is a life-threatening vascular disease associated with blood flow through entry tears in the intima of the native aorta (true lumen, TL) generating a false lumen (FL). Descending aortic dissection (DAD) can be isolated, ie, Stanford type B dissection/Debakey type III (TBAD), or associated with ascending aortic dissection, ie, Stanford type A dissection/Debakey Type I (TAAD). For patients with repaired TAAD (rTAAD), residual chronic DAD (also known as “residual TBAD”) may remain following replacement of the ascending aorta. Treatment planning for DAD is often complex, with the majority of patients initially managed medically with anti-impulse therapy (heart rate and blood pressure control) and interventions such as thoracic endovascular repair (TEVAR) reserved for patients with complications such as rupture and evidence of organ malperfusion.[1–3] The need for invasive treatment for uncomplicated DAD is not well established, as early survival rates for chronic DAD patients on medical therapy are acceptable but long-term outcomes show significant aortic aneurysm formation in 25–50% of patients after 4 years.[4,5] Chronic DAD may require eventual intervention with either open elephant trunk (ET) repair[6,7] or TEVAR, which is less invasive.[8,9]

One of the main questions in chronic DAD is which patients should have TEVAR to prevent complications (aortic rupture, visceral malperfusion). We hypothesize that the comprehensive evaluation of aortic hemodynamics can play a major role in understanding the disease and helping to better classify these patients. Treatment selection for uncomplicated DAD is typically based on clinical findings (ie, symptoms) and simple empirical measures by standard-of-care imaging (eg, maximal aortic diameter and aortic diameter increase)[8] but advancements in blood flow imaging expand our understanding of aortic function. (For instance, FL pressure, driven by locations and sizes of entry and exits tears, as well as the degree of FL thrombus, is critically important in FL remodeling and risk of aorta-related mortality.[10,11] Thus, noninvasive evaluation of FL hemodynamics has the ability to provide unique insight relative to strictly morphologic parameters.) 4D flow magnetic resonance imaging (MRI) (ie, 3D time-resolved phase contrast MRI with 3-directional velocity encoding)[12] is uniquely poised to evaluate complex flow patterns in DAD because of the ability to measure 1) blood flow in all three main directional components, and 2) volumetric coverage to allow for quantitative analysis of the entire aorta. This technique has detected flow alterations in aortic dissection related to aortic dilatation (visualization of helical flow and distal dominant entry tears, quantification of flow velocity in the FL), found substantially higher flow in the TL with FL thrombus, and has been used

to identify small dissection flap fenestrations.[13–17] Previous studies are promising, but were limited by either the utilization of qualitative assessment of flow patterns or localized quantification of hemodynamic metrics, and thus the systematic parameter mapping of flow in the TL and FL is needed.[18,19] Because TL and FL 4D flow-derived metrics may be related to aortic aneurysmal degeneration and FL thrombosis, we developed 4D flow MRI-derived parametric maps of aortic dissection hemodynamics (forward flow, reverse flow, flow stasis, and kinetic energy). The goal of this study was to analyze these parametric maps across different subtypes of chronic descending aorta dissection and compare them to controls.

Materials and Methods

Study Cohort

Aortic 4D flow MRI was acquired in 20 patients (age = 60 ± 11 years; 12 male) with DAD (6 TBAD, 14 rTAAD) and 21 age-matched controls (age = 59 ± 10 years; 13 male). Patients with TBAD were on medical therapy and patients with rTAAD had either already undergone AAo repair (n = 11) or ET stage 1 procedure (ET1) (n = 3) (Table 1). (ET1 is performed by replacing the AAo through the aortic arch, then securing a graft within the descending aorta with plans to subsequently repair the residual DAD through an open or endovascular approach.)

Institutional Review Board approval was obtained for this HIPAA-compliant study. Patients were retrospectively included after 4D flow MRI was performed as part of their standard-of-care MRI between 2012 and 2018. All patients with dissection of the descending thoracic aorta were considered eligible for inclusion, including patients with previous surgical repair. Healthy volunteers were prospectively recruited for research cardiothoracic MRI and written informed consent was obtained from all participants.

Image Acquisition

All images were acquired using 1.5T MR-systems (Avanto, Aera, Siemens Healthcare, Erlangen, Germany) or a 3.0T system (Skyra, Siemens Healthcare). Each subject underwent a free-breathing, prospectively ECG- and respiratory navigator-gated, 4D flow MRI[20] covering the entire thoracic aorta in sagittal oblique orientation. Scan parameters were as follows: spatial resolution = 2.7–5.0 × 2.0–3.1 × 2.2–5.0 mm^3, field of view (FOV) = 340–460 × 238–366 mm^2, slab thickness = 66–130 mm, temporal resolution = 36.8–40.0 msec, repetition time (TR) = 4.6–5.0 msec, echo time (TE) = 2.2–2.5 msec, flip angle = 7–15° and velocity sensitivity (venc) = 150–270 cm/s.

Patients received standard-of-care imaging including simultaneously acquired contrast enhanced time-resolved MR angiogram (MRA) (Ablavar, Gadavist, Magnevist, Bayer Schering Pharma, Berlin, Germany; spatial resolution = 0.9–1.3 × 0.9–1.3 × 80–132 mm^3, temporal resolution = 0.7–1.5 sec, TR = 2.2–2.4 msec, TE = 0.9–1.0 msec, flip angle = 20–25°), available in 16 patients. ECG-gated, contrast enhanced CTA (SOMATOM, Siemens Healthcare; Aquilion, Canon Medical Systems, Tustin, CA; LightSpeed, BrightSpeed, GE Healthcare, Milwaukee, WI; spatial resolution = 0.3–0.9 × 0.3–0.9 × 0.8–5 mm^3) was available in 16 patients within 8 ± 7 months of the MRI.

Data Analysis

The 4D flow MRI data were analyzed according to a previously described preprocessing workflow,[21] ie, corrected for Maxwell terms, eddy currents, noise-masking of areas outside of flow regions, and velocity aliasing.[22,23] Time-averaged magnitude images and a time-averaged 3D phase contrast angiogram (PC-MRA) were calculated to depict vessel anatomy.[24] For controls, the thoracic aorta was segmented from the PC-MRA (Mimics Innovation Suite; Materialise, Leuven, Belgium) and used to mask the 4D flow data. For patients, time-averaged 4D flow magnitude data were used to manually segment the thoracic aorta. Next, the TL was manually segmented based on the PC-MRA data. Subtraction of the TL from the aorta segmentation yielded the FL segmentation. The TL and FL segmentations were used to mask the 4D flow data; see Fig. 1a–e. Contrast-enhanced time-resolved MRA or CTA was referenced to correct for errors.

Parametric Hemodynamic Maps

Maps of aortic hemodynamics were derived based on home-built analysis tools (MatLab; MathWorks, Natick, MA) similar to a recently reported workflow.[25] The 4D flow velocity data were regridded to isotropic 1 mm^3 voxels using spline interpolation. A 3D aortic centerline was calculated and orthogonal planes were automatically placed every millimeter.[26] Each voxel was matched to the nearest plane (ie, having center point at shortest 3D distance) to determine directional flow along the centerline, ie, forward (AAo to DAo) and reverse (ie, DAo to AAo); see Fig. 1f,g. For each voxel inside the TL and FL (DAD patients) or entire aorta (controls), net forward flow (FF) and reverse flow (RF) were calculated as the sum over the cardiac cycle.

The velocity magnitude was determined for each voxel at each cardiac time-frame, ie, $v(t)$. Voxelwise flow stasis was calculated as the percentage of cardiac timeframes with $v(t) <$ 0.10 m/s. In addition, voxelwise kinetic energy (KE) was determined by:

$$KE = \frac{1}{2} \cdot \rho \cdot dV \cdot v(t)^2$$

with ρ the blood density assumed as 1060 kg/m^3 and dV the unit voxel volume (ie, 1 mm^3)[27,28] and summed over the cardiac cycle.

To correct for errors in plane orientation at the beginning and end of the centerline, the first and last four orthogonal planes along the centerline were not included in the directional flow quantifications. To reduce noise, a 3D median 3-by-3-by-3 filter was applied to all voxelwise parameters.

To provide an intuitive visualization of the spatial distribution of hemodynamic parameters across the TL and FL (patients) or entire aorta (controls), anatomic maps for FF, RF, stasis, and KE were calculated. The 3D voxelwise data for each parameter was collapsed into an average intensity projection, ie, average of all voxels in the segmented TL or FL (patients) or aorta (controls) along the projection direction. For quantitative regional analysis, the aorta was separated into five regions of interest (ROIs): 1) AAo (aortic root to brachiocephalic artery); 2) aortic arch (brachiocephalic artery to left subclavian artery); 3) proximal-DAo

(left subclavian artery to vertical DAo); 4) mid-DAo (vertical DAo to half the distance to the celiac trunk); and 5) distal-DAo (distal edge of ROI 4 to the celiac trunk) (Fig. 1h). For each ROI, the mean FF, RF, KE, and flow stasis were quantified. For quantification in the FL, only ROIs containing at least 4000 voxels (=4 mL) were included to ensure a sizeable flow region for quantification.

Interobserver Study

In a subset of subjects, the 4D flow MRI analysis workflow (ie, corrections, vessel segmentation of the TL and FL, drawing of ROIs) was carried out by two independent and blinded observers. This study included eight patients from the cohort (ie, three TBAD, three AAo repair, two ET stage 1).

Statistical Analysis

Metrics of TL and FL hemodynamics were compared between different subject groups (ie, TBAD, AAo repair, ET stage 1, controls) (MatLab). A Lilliefors test was used to assess normality. In the case of normal distribution, an analysis of variance (ANOVA) test was performed and otherwise a Kruskal–Wallis test was used. When $P < 0.05$, paired comparisons between individual groups were conducted using a 2-tailed, unpaired Student's *t*-test (normal distribution) or Wilcoxon Rank tests (non-normal distribution). Correlation and Bland–Altman analysis was performed for the interobserver study. For all analysis $P < 0.05$ was considered statistically significant.

Results

Study Cohort

Patient characteristics are shown in Table 1. Age was not significantly different among the subject groups (ie, TBAD, AAo repair, ET1, controls) ($P = 0.65$). Time since last surgery was not significantly different between the rTAAD groups (ie, AAo repair, ET1) ($P = 0.28$). Two patients in the AAo repair group had comorbidities, ie, one patient had bicuspid aortic valve disease and one patient had Marfan syndrome.

Parametric Hemodynamic 4D Flow MRI Maps

Results for an example subject from each of the three groups (TBAD, rTAAD, and controls) are shown in Fig. 2. Elevated voxelwise forward flow (TL), reverse flow (TL, FL), and kinetic energy (TL) are shown in the patient with AAo repair, compared to the patient with TBAD and the control. Additionally, elevated levels of voxelwise stasis are shown in the patient with TBAD, compared to the patient with AAo repair and the control. These findings indicate a clear difference between the flow characteristics in the rTAAD patient with AAo repair vs. the patient with TBAD (no previous repairs). However, without previous flow imaging it is unknown whether this difference was present before AAo repair.

Results for the entire cohort are given in Figs. 3–5. For global findings, boxplots compare flow parameter results between subject groups for the TL (Fig. 3) and FL (Fig. 4). See also Table 2. For regional findings, schematics of the aorta show results reported separately by

ROI and each section of the aorta is color-coded based on the average value among subjects in the group (Fig. 5).

Parametric Hemodynamic 4D Flow MRI Maps: True Lumen

Global: Patients with rTAAD had elevated TL reverse flow, compared to controls (Fig. 3b) (AAo repair: [85% percent increase in mean value] $P = 0.004$, ET1: [108%] $P = 0.018$). Regional: significant differences in TL reverse flow occurred in the AAo (AAo repair: $P = 0.0002$), arch (AAo repair: $P = 0.004$) and proximal-DAo (AAo repair: $P = 0.005$, ET1: $P = 0.011$) (Fig. 5a).

Global: Patients with rTAAD demonstrated higher TL kinetic energy than controls (AAo repair: [103%] $P = 0.0002$, ET1: [95%] $P = 0.011$) and patients with TBAD (AAo repair: [128%] $P = 0.021$, ET1: [118%] $P = 0.048$) (Fig. 3c). Regional: Significant findings in TL kinetic energy between rTAAD and controls occurred in the AAo (AAo repair: $P = 0.0001$, ET1: $P = 0.045$), arch (AAo repair: $P = 0.0006$, ET1: $P = 0.011$), proximal-DAo (AAo repair: $P = 0.0007$, ET1: $P = 0.007$), and mid-DAo (AAo repair: $P = 0.002$)(Fig. 5b). Also, significant findings in TL kinetic energy between rTAAD and TBAD occurred in the AAo (AAo repair: $P = 0.0025$, ET1: $P = 0.024$), arch (AAo: $P = 0.023$, ET1: $P = 0.048$), and proximal-DAo (AAo: $P = 0.021$, ETA: $P = 0.024$).

Parametric Hemodynamic DAD 4D Flow MRI Maps: False Lumen

Global: Patients with rTAAD had higher FL kinetic energy (AAo repair: [225%] $P = 0.002$, ET1: [138%] $P = 0.024$) and lower FL stasis (AAo repair: [−28%] $P = 0.003$, ET1: [−33%] $P = 0.048$) than patients with TBAD (Figs. 4, 5b,c). Regional: Stasis was markedly elevated throughout the FL in patients with TBAD, while patients with previous AAo repair had reduced FL stasis in the proximal and mid-DAo (TBAD vs. AAo repair: $P = 0.001$, $P = 0.018$) and patients with previous ET1 repair had reduced FL stasis in the distal-DAo (TBAD vs. ET1: $P = 0.048$).

Interobserver Study

The results for correlation and Bland–Altman analysis are shown (Figs. 6, 7). There was only minimal bias between observers for forward flow, reverse flow, stasis, and kinetic energy with low limits of agreement. Analyzing TL and FL results separately, there was a significant bias for TL reverse flow (0.001 ml/cycle [8.2% of average value], $P = 0.01$) with limits of agreement = 0.006 ml/cycle [35%], $r = 0.97$ and slope = 1.1.

Discussion

Quantitative hemodynamic mapping from 4D flow MRI enables characterization of complex flow in the TL and FL of thoracic DAD. Regional flow differences were detected among patients and controls (ie, patients with rTAAD had elevated TL reverse flow and TL kinetic energy) and between patients with rTAAD vs. medically managed TBAD (ie, patients with rTAAD had higher TL and FL kinetic energy and lower FL stasis). This suggests that rTAAD patients tended to have complex flow situations that might lead to aortic complications. However, larger studies and subsequent outcome-related trials are critical to

explore these relationships fully and the potential impact for preventative treatment by TEVAR.

We suspect the elevated flow parameters in rTAAD are the result of prior surgery, but we would need imaging data before dissection (and ideally before intervention, which will be difficult to obtain due to the emergency of treatment in TAAD) to fully assess this. A proposed mechanism is that the difference in KE and retrograde flow after AAo repair might be the result of replacing AAo with a noncompliant graft. Still, these remarks are speculative, and the underlying mechanism will need to be fully explored. Furthermore, it remains unclear whether the elevated flow metrics in patients with TAAD will lead to higher rates of aneurysm.[10,29] Thus, it will be useful to follow patients with rTAAD over time to monitor the effects of elevated flow parameters on aortic size and rate of complications such as aortic aneurysmal degeneration and failure of FL thrombosis.

Reverse flow can occur in the TL even when aortic regurgitation is not present due to complex flow (ie, circling of flow and/or flow between the TL and FL via intimal entry tears). This “regional” type of flow reversal can be captured using the voxelwise reverse flow quantification utilized here (instead of plane-based, which may miss important regional flow information).

Similar to our study, a recent 4D flow MRI study of 10 chronic DAD patients after AAo repair[16] found high levels of slow flow in the FL compared to the TL and normal aorta. However, they found lower overall flow profiles and no differences in flow reversal in the TL of patients, compared to controls. The controls were not age-matched to the patients (controls were on average 18 years younger than patients), which may help explain some of these differences. But more likely, this is the result of inherent flow variations in rTAAD (seen also in our study), probably influenced by the success of surgery to treat intimal entry in the AAo and aortic arch and thus providing evidence of the importance to study individual complex flow situations postrepair. This relationship between entry or re-entry size and flow in TL and FL is already reported by a 4D flow MRI study on 16 patients with abdominal aortic dissection, the intimal entry size being positively correlated with FL net and peak flow, when FL thrombosis was associated with high velocity in the TL.[15] Our results are also in agreement with a recent in vitro and in vivo study involving 14 DAD patients, seven with rTAAD (with prior AAo surgery) and seven with TBAD, who found similar results in terms of difference in forward flow and backward flow between TL and FL (not using parametric mapping) with a good reproducibility; however, there was no comparison between the type of AD.[30] In a recent study of 139 patients after TEVAR,[31] chronic vs. acute DAD, rather than TBAD vs. rTAAD, impacted the procedure success. Nevertheless, since choice of indication in asymptomatic patients and TEVAR procedure remains challenging, the results may improve if 4D flow MRI data are used to predict post TEVAR hemodynamics[32] and subsequently monitor the results.[33] Thus, hemodynamic mapping throughout the stages of disease progression, as well as pre- and post-surgery, will be an important next step in the understanding and improvement of risk-stratification.

This study has limitations. The patient cohort was small and heterogeneous in nature. The size of the communication between the FL and TL was variable and impacted by both

surgical technique and patient anatomy. Further work with larger populations and follow-up may help identify hemodynamic features that improve risk-stratification and their relationship or incremental value against standard imaging features like aortic diameter as well as the size and localization of re-entry tears. The number of rTAAD patients with ET stage 1 was only three, but due to having largely different etiology and surgical repair from the AAo repair group, they were considered separately. While this presented limitations in the statistical analysis, it provided initial insights into the hemodynamics of ET stage 1, which ultimately did show a tendency to align with AAo repair but also showed some values out-of-range (eg, FL reverse flow, FL stasis). In addition, the ET stage 1 patient group was entirely male. Since differences have been found in normal aortic hemodynamics (eg, peak velocity) between genders,[34] we suggest larger future prospective studies with better gender distribution. Segmentation of aortic dissection remains challenging and contributed to the variation between observers in this study. In addition, determining the mid-DAo segment was some-what variable, as there were not clear anatomical landmarks such as aortic branches to define the ROI. Nevertheless, the observers were still in relatively good agreement. However, reproducibility could be improved by 1) utilizing high blood-tissue contrast anatomical imaging registered to flow data for segmentation, and 2) exploring machine-learning algorithms to segment the dissection and determine ROIs. We used a time-averaged segmentation, which may lead to suboptimal segmentation due to motion through the cardiac cycle of the intimal flap, but interpretation of the parametric map may be less influenced by this segmentation. The voxelwise values that we reported in this study were not normalized to arterial pressure, cardiac output, or medication therapies and we anticipate that these could affect flow parameters such as KE. It will be useful in future studies to monitor these clinical values and study their relationship with hemodynamics.

In conclusion, this study demonstrates the utility of hemodynamic mapping from 4D flow MRI as a quantitative technique for the characterization of chronic DAD, showing differences between rTAAD and TBAD in descending aorta TL and FL flow patterns. These results indicate the potential for parametric mapping of underlying hemodynamics in the TL and FL (directional flow, flow stasis, kinetic energy) to play an important role in the understanding of aortic dissection. Future studies are warranted to determine key metrics related to outcome, help to plan invasive procedures, and monitor asymptomatic patients over time.

Acknowledgments

Contract grant sponsor: National Institutes of Health, National Heart, Lung and Blood Institute (NHLBI); Contract grant number: T32HL134633.

References

1. Tran TP, Khoynezhad A. Current management of type B aortic dissection. Vasc Health Risk Manag 2009;5:53–63. [PubMed: 19436678]
2. Suzuki T, Mehta RH, Ince H, et al. Clinical profiles and outcomes of acute type B aortic dissection in the current era: Lessons from the International Registry of Aortic Dissection (IRAD). Circulation 2003;108 (Suppl 1):II312–317. [PubMed: 12970252]

3. Riambau V, Bockler D, Brunkwall J, et al. Editor's Choice — Management of descending thoracic aorta diseases: Clinical practice guidelines of the European Society for Vascular Surgery (ESVS). Eur J Vasc Endovasc Surg 2017;53:4–52. [PubMed: 28081802]
4. Luebke T, Brunkwall J. Type B aortic dissection: A review of prognostic factors and meta-analysis of treatment options. Aorta 2014;2:265–278. [PubMed: 26798745]
5. Coady MA, Ikonomidis JS, Cheung AT, et al. Surgical management of descending thoracic aortic disease: Open and endovascular approaches: A scientific statement from the American Heart Association. Circulation 2010;121:2780–2804. [PubMed: 20530003]
6. Nienaber CA, Divchev D, Palisch H, Clough RE, Richartz B. Early and late management of type B aortic dissection. Heart 2014;100:1491–1497. [PubMed: 25092877]
7. Borst HG, Walterbusch G, Schaps D. Extensive aortic replacement using "elephant trunk" prosthesis. Thorac Cardiovasc Surg 1983;31:37–40. [PubMed: 6189250]
8. Fattori R, Montgomery D, Lovato L, et al. Survival after endovascular therapy in patients with type B aortic dissection: A report from the International Registry of Acute Aortic Dissection (IRAD). JACC Cardiovasc Intervent 2013;6:876–882.
9. Nienaber CA, Kische S, Rousseau H, et al. Endovascular repair of type B aortic dissection: Long-term results of the randomized investigation of stent grafts in aortic dissection trial. Circ Cardiovasc Intervent 2013;6:407–416.
10. Evangelista A, Salas A, Ribera A, et al. Long-term outcome of aortic dissection with patent false lumen: Predictive role of entry tear size and location. Circulation 2012;125:3133–3141. [PubMed: 22615344]
11. Tsai TT, Evangelista A, Nienaber CA, et al. Partial thrombosis of the false lumen in patients with acute type B aortic dissection. N Engl J Med 2007;357:349–359. [PubMed: 17652650]
12. Dyverfeldt P, Bissell M, Barker AJ, et al. 4D flow cardiovascular magnetic resonance consensus statement. J Cardiovasc Magn Reson 2015; 17:72. [PubMed: 26257141]
13. Clough RE, Waltham M, Giese D, Taylor PR, Schaeffter T. A new imaging method for assessment of aortic dissection using four-dimensional phase contrast magnetic resonance imaging. J Vasc Surg 2012;55:914–923. [PubMed: 22386146]
14. Francois CJ, Markl M, Schiebler ML, et al. Four-dimensional, flow-sensitive magnetic resonance imaging of blood flow patterns in thoracic aortic dissections. J Thorac Cardiovasc Surg 2013;145:1359–1366. [PubMed: 22841438]
15. Liu D, Fan Z, Li Y, et al. Quantitative study of abdominal blood flow patterns in patients with aortic dissection by 4-dimensional flow MRI. Sci Rep 2018;8:9111. [PubMed: 29904131]
16. Sherrah AG, Callaghan FM, Puranik R, et al. Multi-velocity encoding four-dimensional flow magnetic resonance imaging in the assessment of chronic aortic dissection. Aorta 2017;5:80–90. [PubMed: 29675440]
17. Allen BD, Aouad PJ, Burris NS, et al. Detection and hemodynamic evaluation of flap fenestrations in type B aortic dissection with 4D flow MRI: Comparison with conventional MRI and CT angiography. Radiol Cardiothor Imaging 2019;1:e180009.
18. Baliga RR, Nienaber CA, Bossone E, et al. The role of imaging in aortic dissection and related syndromes. JACC Cardiovasc Imaging 2014;7: 406–424. [PubMed: 24742892]
19. Trimarchi S, Tolenaar JL, Jonker FH, et al. Importance of false lumen thrombosis in type B aortic dissection prognosis. J Thorac Cardiovasc Surg 2013;145(3 Suppl):S208–212. [PubMed: 23260434]
20. Markl M, Harloff A, Bley TA, et al. Time-resolved 3D MR velocity mapping at 3T: Improved navigator-gated assessment of vascular anatomy and blood flow. J Magn Reson Imaging 2007;25:824–831. [PubMed: 17345635]
21. Schnell S, Entezari P, Mahadewia RJ, et al. Improved semiautomated 4D flow MRI analysis in the aorta in patients with congenital aortic valve anomalies versus tricuspid aortic valves. J Comput Assist Tomogr 2016; 40:102–108. [PubMed: 26466113]
22. Bernstein MA, Zhou XJ, Polzin JA, et al. Concomitant gradient terms in phase contrast MR: Analysis and correction. Magn Reson Med 1998;39: 300–308. [PubMed: 9469714]

23. Walker PG, Cranney GB, Scheidegger MB, Waseleski G, Pohost GM, Yoganathan AP. Semiautomated method for noise reduction and background phase error correction in MR phase velocity data. J Magn Reson Imaging 1993;3:521–530. [PubMed: 8324312]
24. Bock J, Kreher BW, Hennig J, Markl M. Optimized pre-processing of time-resolved 2D and 3D phase contrast MRI data. In: Proc 15th Annual Meeting ISMRM, Berlin; 2007 Abstract 3138.
25. Shen X, Schnell S, Barker AJ, et al. Voxel-by-voxel 4D flow MRI-based assessment of regional reverse flow in the aorta. J Magn Reson Imaging 2018;47:1276–1286. [PubMed: 28925047]
26. Vali A, Aristova M, Vakil P, et al. Semi-automated analysis of 4D flow MRI to assess the hemodynamic impact of intracranial atherosclerotic disease. Magn Reson Med 2019;28:27747.
27. Chandran KB, Yoganathan AP, Rittgers SE. Biofluid mechanics: The human circulation. London: Taylor & Francis Group; 2007.
28. Cibis M, Bustamante M, Eriksson J, Carlhall CJ, Ebbers T. Creating hemodynamic atlases of cardiac 4D flow MRI. J Magn Reson Imaging 2017;46:1389–1399. [PubMed: 28295788]
29. Oda T, Minatoya K, Sasaki H, et al. Surgical indication for chronic aortic dissection in descending thoracic and thoracoabdominal aorta. Circ Cardiovasc Intervent 2017;10(2).
30. de Beaufort HW, Shah DJ, Patel AP, et al. Four-dimensional flow cardiovascular magnetic resonance in aortic dissection: Assessment in an ex vivo model and preliminary clinical experience. J Thorac Cardiovasc Surg 2019;157:467–476 e461. [PubMed: 30121136]
31. Pantaleo A, Jafrancesco G, Buia F, et al. Distal stent graft-induced new entry: An emerging complication of endovascular treatment in aortic dissection. Ann Thorac Surg 2016;102:527–532. [PubMed: 27112653]
32. Pirola S, Guo B, Menichini C, et al. 4D Flow MRI-based computational analysis of blood flow in patient-specific aortic dissection. IEEE Trans Biomed Eng 2019 [Epub ahead of print].
33. Takei Y, Itatani K, Miyazaki S, Shibasaki I, Fukuda H. Four-dimensional flow magnetic resonance imaging analysis before and after thoracic endovascular aortic repair of chronic type B aortic dissection. Interact Cardiovasc Thorac Surg 2019;28:413–420. [PubMed: 30239771]
34. Garcia J, van der Palen RLF, Bollache E, et al. Distribution of blood flow velocity in the normal aorta: Effect of age and gender. J Magn Reson Imaging 2018;47:487–498. [PubMed: 28556277]

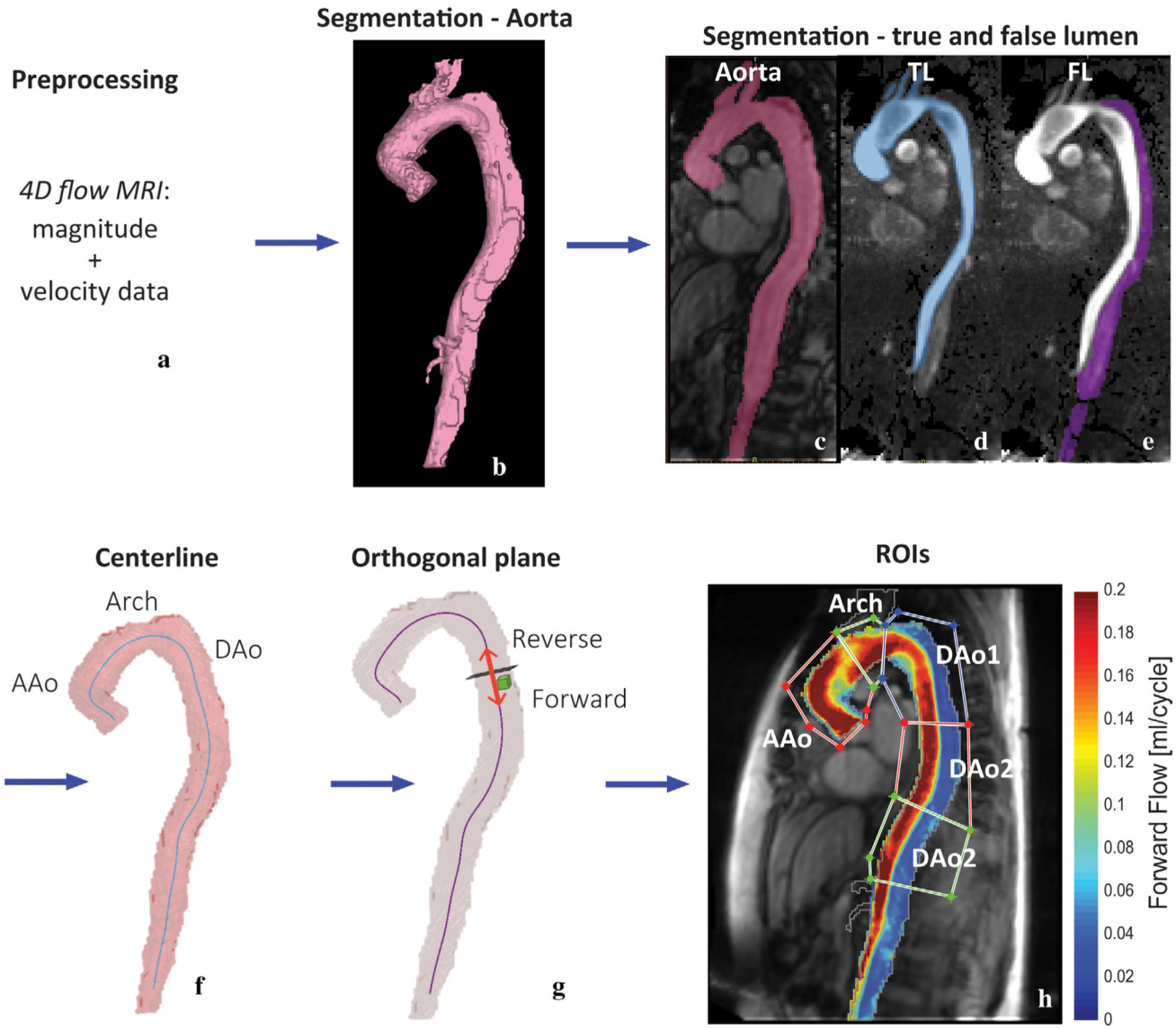

FIGURE 1:

Data analysis workflow. (a) Preprocessing of the original 4D flow data included calculation of time-averaged magnitude images and a 3D phase-contrast MR angiogram (PC-MRA) enabling (b) 3D segmentation of the thoracic aorta (ie, extending from the aortic trunk to celiac arteries), and (c–e) separation of TL (ie, depicted by 3D PC-MRA) and FL (ie, depicted by time-averaged magnitude images). (f) Automatic calculation of 3D centerline allowed for (g) voxelwise definition of flow direction, ie, forward (AAo to DAo) and reverse flow (DAo to AAo), based on the closest orthogonal plane. (h) Average intensity map with five ROIs defined for quantification.

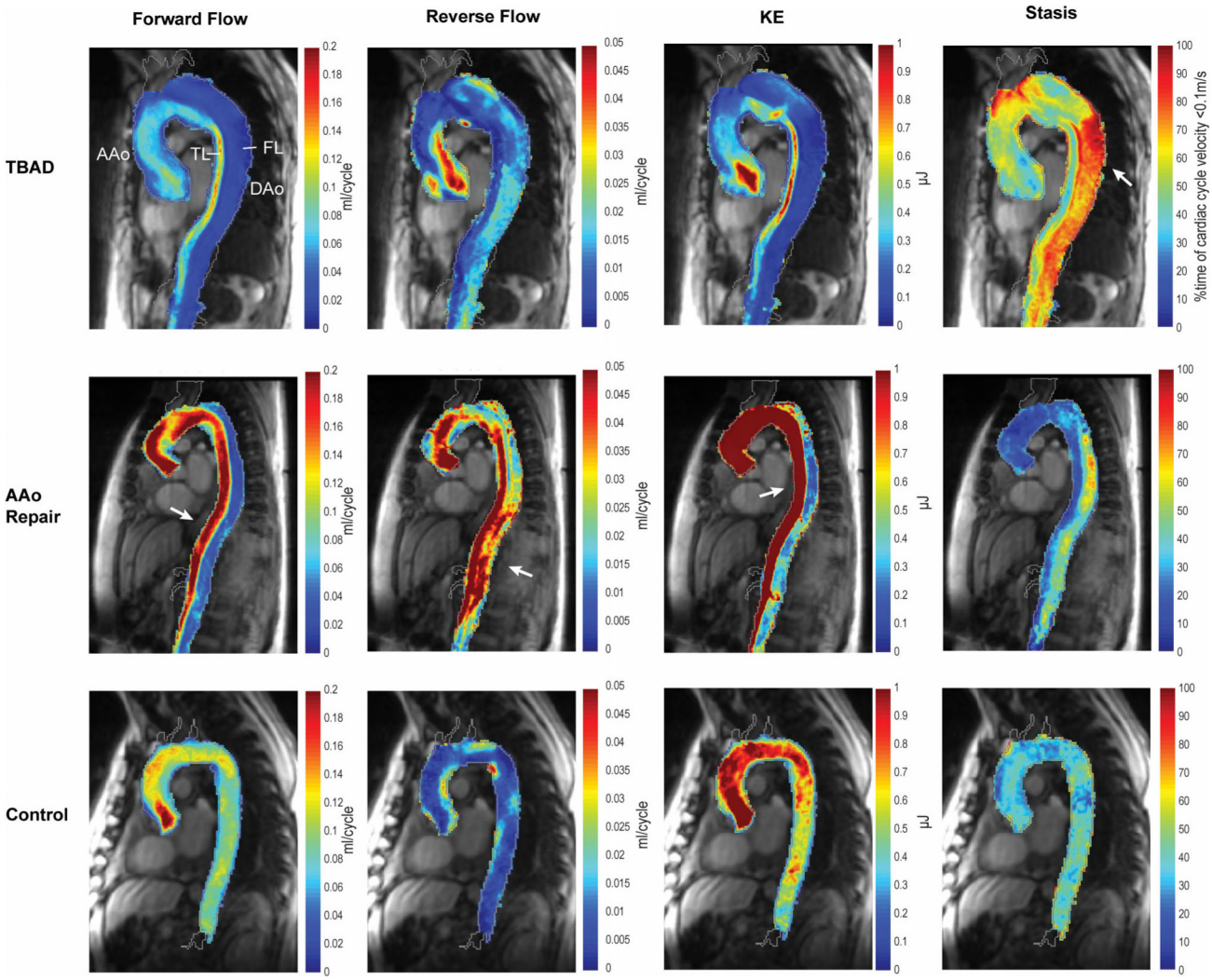

FIGURE 2:

Forward flow, reverse flow, kinetic energy and stasis maps in three example subjects. Top: A 55-year-old medically managed TBAD patient; middle: a 63-year-old patient with rTAAD after open AAo replacement with aortic valve replacement; and bottom: a 54-year-old control. White arrows show regions of elevated forward flow, reverse flow, and kinetic energy (patient with AAo repair) as well as elevated stasis (patient with TBAD).

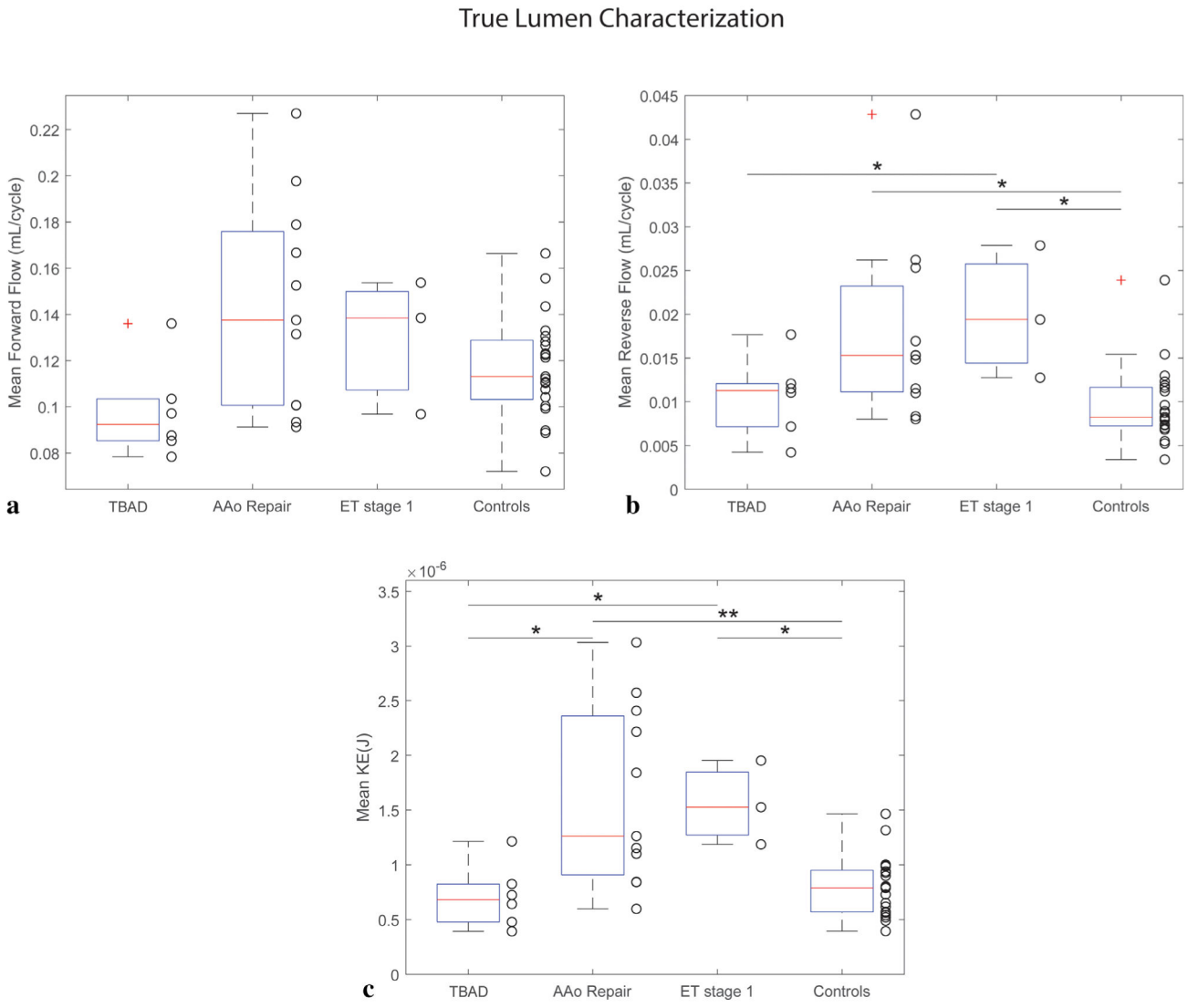

FIGURE 3:

Hemodynamic characterization of the true lumen in patients with aortic dissection. Boxplot is shown with red line = median, large box = [25, 75]% of data. Each datapoint represents the average ROI value for one subject along the TL (for patients) or entire aorta (for controls). *$P < 0.05$, **$P < 0.001$. KE: kinetic energy.

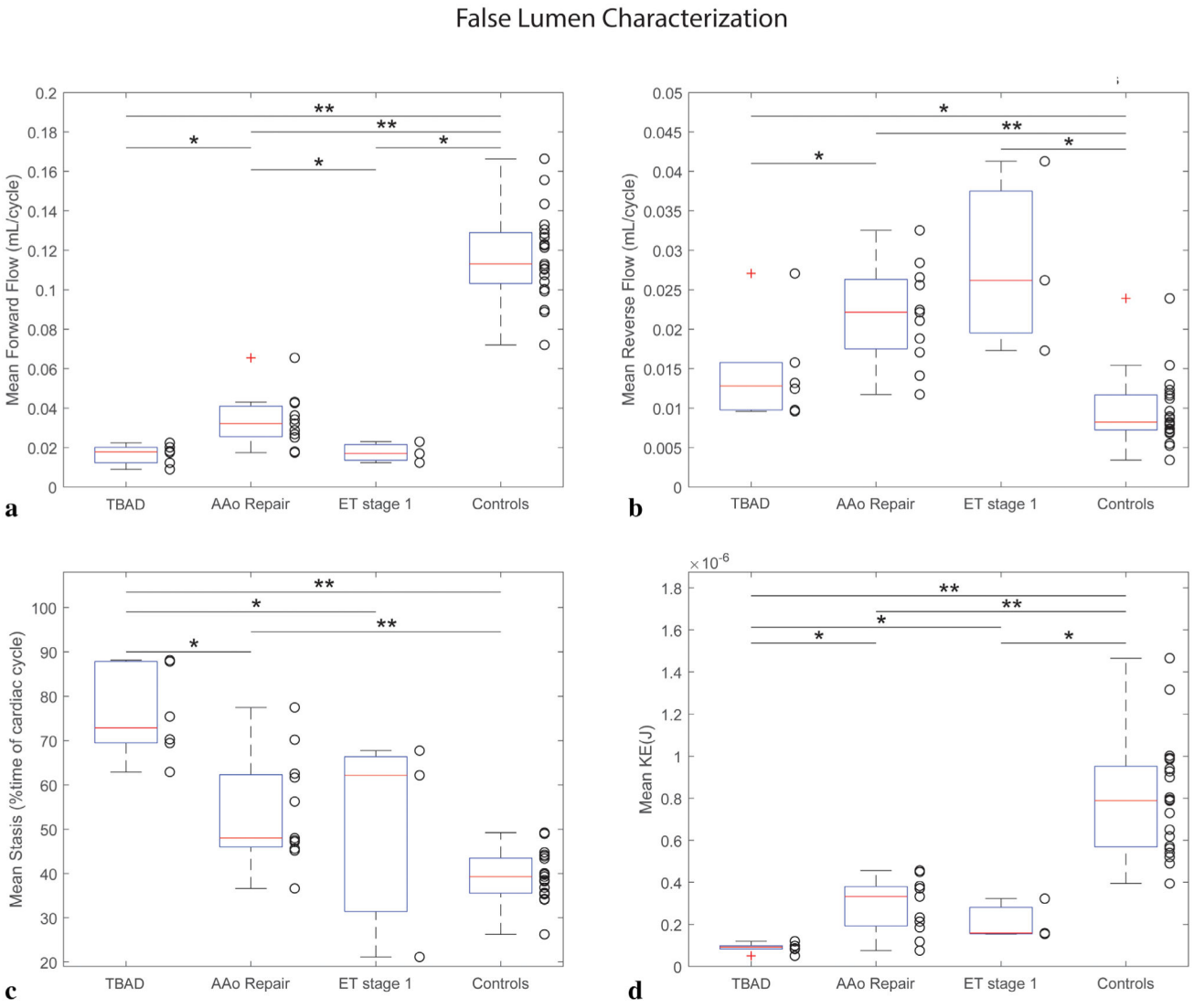

FIGURE 4:

Hemodynamic characterization of the false lumen in patients with aortic dissection. Boxplot is shown with red line = median, large box = [25, 75]% of data. Each datapoint represents the average ROI value for one subject along the FL (for patients) or entire aorta (for controls). *$P < 0.05$, **$P < 0.001$. KE: kinetic energy.

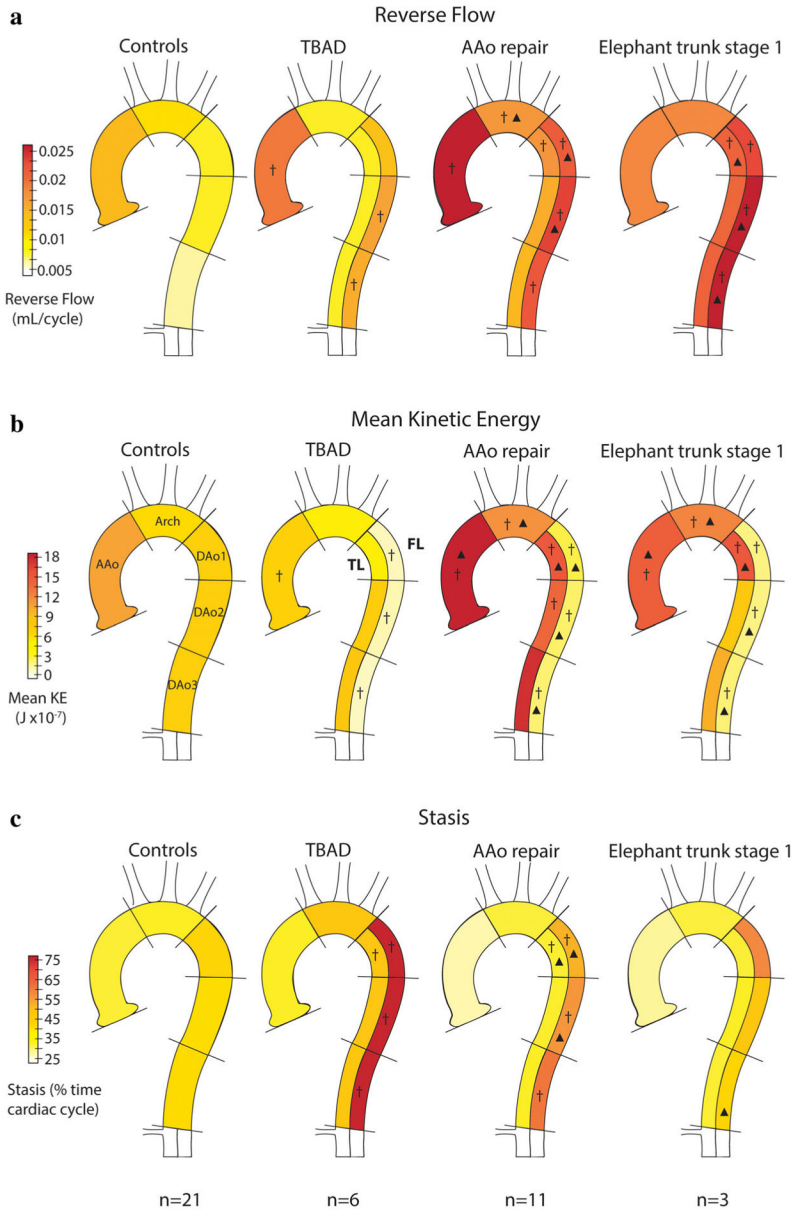

FIGURE 5:

Regional analysis results. Schematic of aortic hemodynamics for ROIs in the TL and FL for patients with medically managed TBAD and rTAAD (ie, after AAo repair or ET stage 1). For comparison, results in aorta of healthy controls are shown on the left. Note, color-coding illustrates elevated values of reverse flow, KE, and stasis. Symbols indicate significant *P*-values: † = $P < 0.05$ compared to controls, ▲ = $P < 0.05$ compared to TBAD.

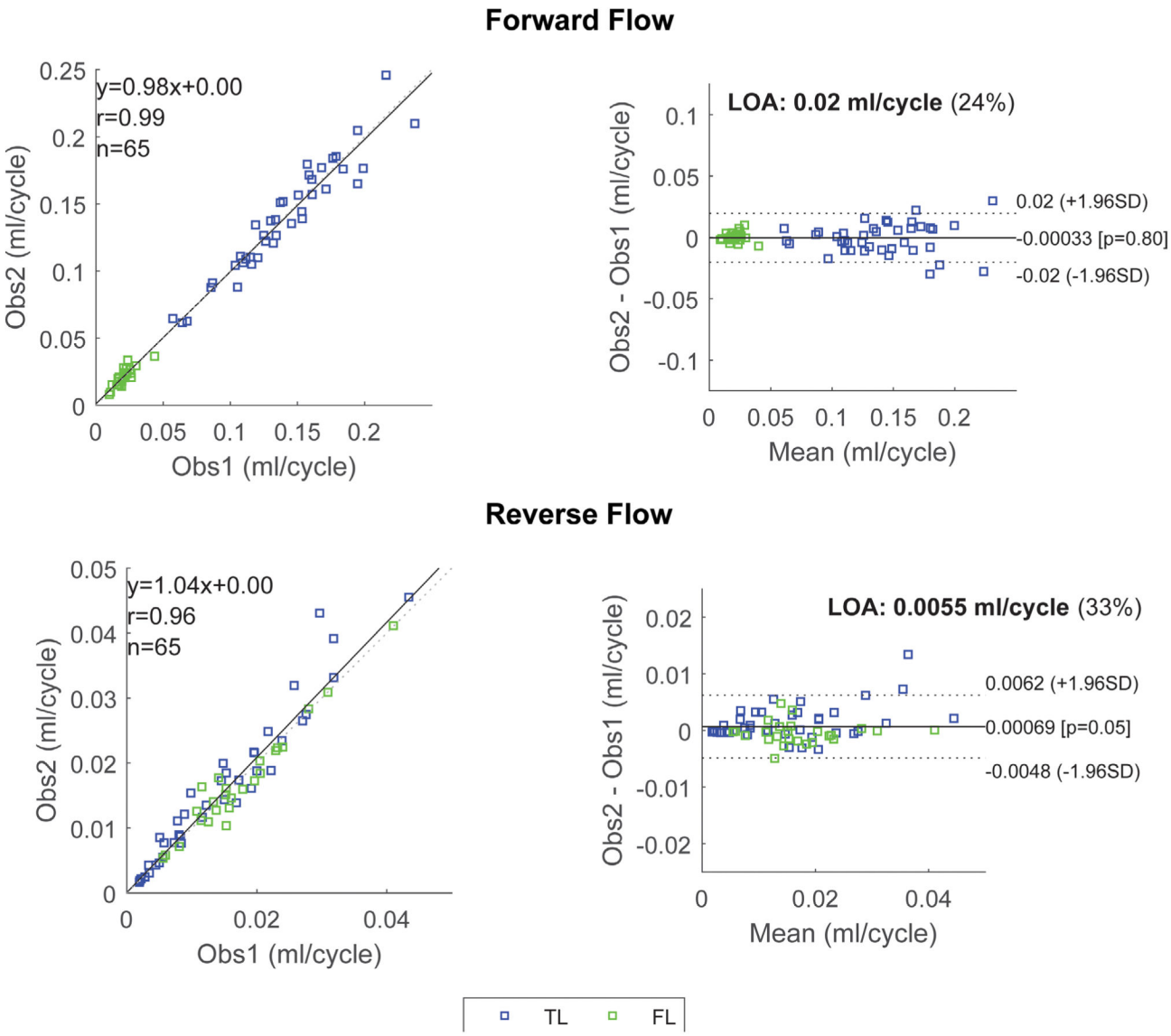

FIGURE 6:
Interobserver study correlation and Bland–Altman plots for forward and reverse flow.

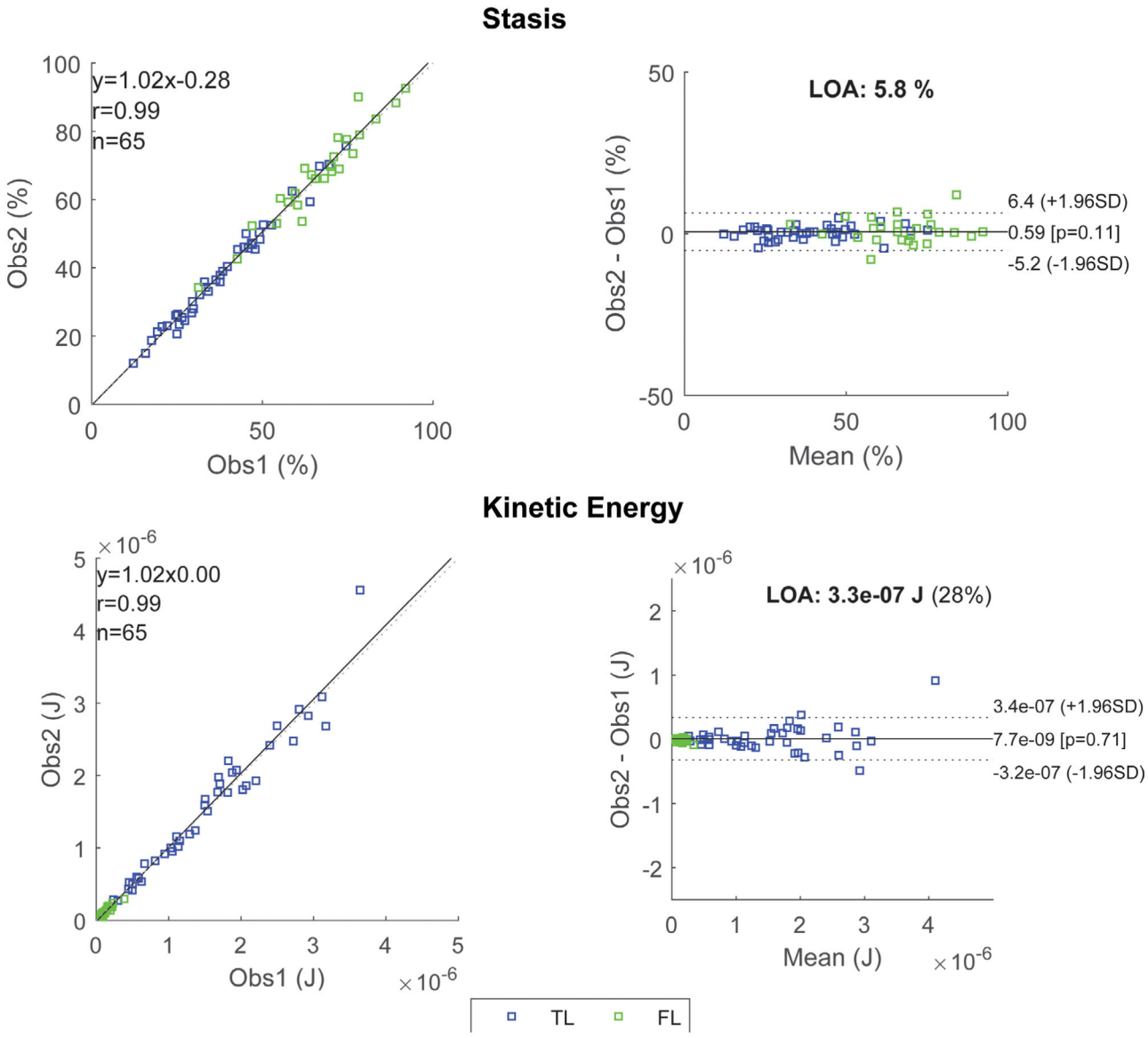

FIGURE 7:
Interobserver study correlation and Bland–Altman plots for stasis and kinetic energy.

TABLE 1.

Patient Characteristics and Surgical History

Group	*n*	Age, in years	Male sex, no. (%)	Months since last procedure
TBAD	6	62 ± 8 [54–76]	2 (33%)	n/a
rTAAD				
AAo repair	11	60 ± 13 [35–86]	7 (64%)	34 ± 51 [4–156]
ET stage 1	3	55 ± 1 [54–56]	3 (100%)	7 ± 6 [0.1–13]
Prior surgeries for patients with AAo Repair				
Open AAo replacement with AV replacement				
Bentall procedure, open AAo replacement, total arch repair				
Open AAo replacement with AV resuspension				
Open valve-sparing AAo replacement, AV resuspension				
AV replacement, open valve-sparing AAo replacement, hemiarch reconstruction				
Hemiarch reconstruction				
Open valve-sparing root replacement with AAo repair				
Bentall procedure, AAo reconstruction, CABG, open thoracic DAo replacement				
Valve-sparing aortic root replacement				
Open AAo replacement with hemiarch reconstruction, Biobentall procedure with total arch reconstruction				
Aortic arch reconstruction				
Prior surgeries for patients with ET stage 1				
MVR, open valve-sparing AAo replacement, total arch reconstruction, ET stage 1 procedure				
Open AAo replacement, AV resuspension, hemiarch reconstruction; Bentall procedure, total arch reconstruction, frozen ET stage 1 procedure				
AAo replacement, AV resuspension, Aortic root and total arch reconstruction, ET stage 1 procedure				

AAo = ascending aorta; AV = aortic valve; CABG = coronary artery bypass graft; ET = elephant trunk; MV = mitral valve; TBAD = type B aortic dissection; rTAAD = repaired type A aortic dissection.

TABLE 2.

Voxelwise Hemodynamic Parameter Results for All Groups

Parameter	1: TBAD	2: AAo repair	3: ET1	4: Controls	*P* (overall)	*P* (1&2)	*P* (1&3)	*P* (1&4)	*P* (2&3)	*P* (2&4)	*P* (3&4)
Forward Flow FL [ml/cycle]	0.017 ± 0.005	0.034 ± 0.014	0.017	0.117 ± 0.022	0.000 *	0.010 *	0.905	0.000 *	0.022 *	0.000 *	0.007 *
Forward Flow TL [ml/cycle]	0.098 ± 0.021	0.143 ± 0.046	0.130		0.062						
Kinetic Energy FL [μJ]	0.089 ± 0.023	0.290 ± 0.131	0.212	0.799 ± 0.269	0.000 *	0.002 *	0.024 *	0.000 *	0.291	0.000 *	0.007 *
Kinetic Energy TL [μJ]	0.713 ± 0.292	1.625 ± 0.825	1.555		0.001 *	0.021 *	0.048 *	0.501	0.885	0.000 *	0.011 *
Reverse Flow FL [ml/cycle]	0.015 ± 0.007	0.022 ± 0.006	0.028	0.010 ± 0.004	0.000 *	0.040 *	0.095	0.034 *	0.456	0.000 *	0.009 *
Reverse Flow TL [ml/cycle]	0.011 ± 0.005	0.018 ± 0.010	0.020		0.007 *	0.180	0.048 *	0.622	0.456	0.004 *	0.018 *
Stasis FL [%]	75.7 ± 10.3	54.4 ± 12.3	50.3	39.2 ± 5.4	0.000 *	0.003 *	0.048 *	0.000 *	1.000	0.000 *	0.383

Results are reported as mean ± standard deviation.

Standard deviation was not included for ET1 group with $n = 3$ patients.

True lumen (TL) and false lumen (FL) parameters in patients were compared to normal values in controls.

* $P < 0.05$.